

# Surface-assisted carrier excitation in plasmonic nanostructures

Tigran V. Shahbazyan

*Department of Physics, Jackson State University, Jackson, MS 39217 USA*

We present a quantum-mechanical model for surface-assisted carrier excitation by optical fields in plasmonic nanostructures of arbitrary shape. We derive an explicit expression, in terms of local fields inside the metal structure, for surface absorbed power and surface scattering rate that determine the enhancement of carrier excitation efficiency near the metal-dielectric interface. We show that surface scattering is highly sensitive to the local field polarization, and can be incorporated into metal dielectric function along with phonon and impurity scattering. We also show that the obtained surface scattering rate describes surface-assisted plasmon decay (Landau damping) in nanostructures larger than the nonlocality scale. Our model can be used for calculations of plasmon-assisted hot carrier generation rates in photovoltaics and photochemistry applications.

## I. INTRODUCTION

Plasmon-assisted hot carrier excitation and transfer across the interfaces [1] has recently attracted intense interest due to wide-ranging applications in photovoltaics [2–11] and photochemistry [12–16]. In metal nanostructures with characteristic size  $L$  below the diffraction limit, i.e.,  $L < c/\omega$ , where  $c$  and  $\omega$  are, respectively, the light speed and frequency, the light scattering is relatively weak, and the absorption is dominated by resonant excitation of surface plasmons, which subsequently decay into electron-hole ( $e$ - $h$ ) pairs through several decay mechanisms depending on the size and shape of a plasmonic system [17–21]. While in relatively large systems, excitation of  $e$ - $h$  pairs with optical energy  $\hbar\omega$  is accompanied by momentum relaxation due to phonon and impurity scattering, for systems with characteristic size  $L \sim 20$  or smaller, the dominant momentum relaxation channel is surface scattering that leads, in particular, to size and shape dependence of the plasmon linewidth [22–32]. Calculations of surface-assisted decay rate have been performed for some simple shapes (mostly spherical) within random phase approximation (RPA) [33–41] or time-dependent local density approximation (TDDFT) [42–48] approaches, while for general shape systems, the classical scattering model [49–53] suggested the surface scattering rate in the form  $\gamma_{cs} = Av_F/L_s$ , where  $L_s$  is the ballistic electron scattering length, and the constant  $A$  includes the effects of surface potential, electron spillover, and dielectric environment [54]. Note, however, that recent measurements of plasmon linewidth in nanostructures of various shapes revealed significant discrepancies with a simple  $L^{-1}$  dependence [27, 30–32].

Here we present a quantum-mechanical model for surface-assisted excitation of  $e$ - $h$  pairs by alternating local electric field of the form  $\mathbf{E}(\mathbf{r})e^{-i\omega t}$  created in the metal either by excitation of a plasmon or as a response to monochromatic external field. We show that surface contribution to the absorbed power due to energy transfer to the excited carriers is given by

$$Q_s = \frac{e^2}{2\pi^2\hbar} \frac{E_F^2}{(\hbar\omega)^2} \int dS |E_n|^2, \quad (1)$$

where integration is taken over the metal surface,  $E_n$  is the local field component *normal* to the interface, and  $E_F$  is the Fermi energy in the metal. The above expression, which is derived within RPA approach, is valid for systems of arbitrary shape that are significantly larger than the nonlocality scale  $v_F/\omega$  [55, 56], i.e., for systems at least several nm large. We compute the surface enhancement of the carrier excitation efficiency for some common nanostructures and show that it is highly sensitive to the local field polarization and system geometry.

## II. THEORY

We consider a metal nanostructure characterized by complex dielectric function  $\varepsilon(\omega) = \varepsilon'(\omega) + i\varepsilon''(\omega)$  in a medium with dielectric constant  $\varepsilon_d$ , and, for simplicity, restrict ourselves by systems with a single metal-dielectric interface. The standard expression for absorbed power has the form [57],

$$Q = \frac{\omega\varepsilon''(\omega)}{8\pi} \int dV |\mathbf{E}|^2. \quad (2)$$

where integration is carried over the metal volume, while the local field  $\mathbf{E}(\mathbf{r})$  is determined, in the quasistatic limit, by the Gauss's law  $\nabla[\varepsilon'(\omega, \mathbf{r})\mathbf{E}(\mathbf{r})] = 0$  [here  $\varepsilon(\omega, \mathbf{r})$  equals  $\varepsilon(\omega)$  and  $\varepsilon_d$  in the metal and dielectric regions, respectively]. The surface contribution to the absorbed power is  $Q_s = \hbar\omega/\tau$ , where  $1/\tau$  is the first-order transition probability rate, leading to the standard RPA expression [41]

$$Q_s = \pi\omega \sum_{\alpha\beta} |M_{\alpha\beta}|^2 [f(\epsilon_\alpha) - f(\epsilon_\beta)] \delta(\epsilon_\alpha - \epsilon_\beta + \hbar\omega). \quad (3)$$

Here,  $M_{\alpha\beta} = \int dV \psi_\alpha^* \Phi \psi_\beta$  is the matrix element of local potential  $\Phi(\mathbf{r})$  defined as  $e\mathbf{E} = -\nabla\Phi$  ( $e$  is the electron charge),  $\psi_\alpha(\mathbf{r})$  and  $\psi_\beta(\mathbf{r})$  are wave-functions for electron states with energies  $\epsilon_\alpha$  and  $\epsilon_\beta$ , respectively, separated by  $\hbar\omega$ , and  $f(\epsilon)$  is the Fermi distribution function. For nanostructures of arbitrary shape, numerical evaluation of  $M_{\alpha\beta}$  is a highly complicated task due to the complexity of electron wave functions. However, as we show below,

for the hard-wall confining potential,  $Q_s$  can be derived in a closed form for any system significantly larger than  $v_F/\omega$  (but still smaller than  $c/\omega$ ).

Excitation of an  $e$ - $h$  pair with a large, compared to the electron level spacing, energy  $\hbar\omega$  requires momentum transfer to the cavity boundary. We note that the boundary contribution to  $M_{\alpha\beta}$  can be presented as an integral over the metal surface [58],

$$M_{\alpha\beta}^s = \frac{-e\hbar^4}{2m^2\epsilon_{\alpha\beta}^2} \int dS [\nabla_n \psi_\alpha(\mathbf{s})]^* E_n(\mathbf{s}) \nabla_n \psi_\beta(\mathbf{s}), \quad (4)$$

where  $\nabla_n \psi_\alpha(\mathbf{s})$  is the wave function derivative normal to the surface,  $E_n(\mathbf{s})$  is the corresponding normal field component,  $\epsilon_{\alpha\beta} = \epsilon_\alpha - \epsilon_\beta$  is the  $e$ - $h$  pair excitation energy, and  $m$  is the electron mass. Using this matrix element, Eq. (3) takes the form

$$Q_s = \frac{e^2\hbar^4}{4\pi m^4 \omega^3} \iint dS dS' E_n(\mathbf{s}) E_n^*(\mathbf{s}') F_\omega(\mathbf{s}, \mathbf{s}'), \quad (5)$$

where  $F_\omega(\mathbf{s}, \mathbf{s}')$  is the  $e$ - $h$  surface correlation function,

$$F_\omega(\mathbf{s}, \mathbf{s}') = \int d\epsilon f_\omega(\epsilon) \rho_{nn'}(\epsilon; \mathbf{s}, \mathbf{s}') \rho_{n'n}(\epsilon + \hbar\omega; \mathbf{s}', \mathbf{s}), \quad (6)$$

defined in terms of normal derivative of the electron cross density of states,  $\rho(\epsilon; \mathbf{s}, \mathbf{s}') = \text{Im}G(\epsilon; \mathbf{s}, \mathbf{s}')$ , at surface points:  $\rho_{nn'}(\epsilon; \mathbf{s}, \mathbf{s}') = \nabla_n \nabla_{n'} \text{Im}G(\epsilon; \mathbf{s}, \mathbf{s}')$ . Here  $G(\epsilon; \mathbf{s}, \mathbf{s}')$  is the confined electron Green function, and the function  $f_\omega(\epsilon) = f(\epsilon) - f(\epsilon + \hbar\omega)$  restricts the initial energy of promoted electron to the interval  $\hbar\omega$  below  $E_F$ .

To evaluate  $Q_s$ , we note that excitation of an  $e$ - $h$  pair with energy  $\hbar\omega$  is accompanied by momentum transfer  $\sim \hbar\omega/v_F$  and, hence, takes place in a region of size  $\sim v_F/\omega$ , so that the  $e$ - $h$  correlation function  $F_\omega(\mathbf{s}, \mathbf{s}')$  peaks in the region  $|\mathbf{s} - \mathbf{s}'| \lesssim v_F/\omega$  and rapidly oscillates outside of it (see below). At the same time, the local fields significantly change on a much larger scale  $\sim L$ . Therefore, for  $L \gg v_F/\omega$ , the main contribution to the integral in Eq. (5) comes from the regions with  $E_n(\mathbf{s}) \approx E_n(\mathbf{s}')$ , so that  $Q_s$  takes the form

$$Q_s = \frac{e^2\hbar^4}{4\pi m^4 \omega^3} \int dS |E_n(\mathbf{s})|^2 \bar{F}_\omega(\mathbf{s}), \quad (7)$$

where  $\bar{F}_\omega(\mathbf{s}) = \int dS' F_\omega(\mathbf{s}, \mathbf{s}')$ . Evaluation of  $\bar{F}_\omega$  is based upon multiple-reflection expansion for the electron Green function  $G(\epsilon; \mathbf{s}, \mathbf{s}')$  in a hard-wall cavity [59]. For system's characteristic size  $L \gg \lambda_F$ , where  $\lambda_F$  is the Fermi wavelength, the main contribution comes from the direct and singly-reflected paths, while the higher-order reflections are suppressed as powers of  $\lambda_F/L$ . In the leading order, we obtain  $G(\epsilon; \mathbf{s}, \mathbf{s}') = 2G_0(\epsilon, \mathbf{s} - \mathbf{s}')$ , where  $G_0(\epsilon, r) = (m/2\pi\hbar^2) e^{ik_\epsilon r}/r$ , with  $k_\epsilon = \sqrt{2m\epsilon}/\hbar$ , is the free electron Green function and factor 2 comes from equal contributions of the direct and singly-reflected paths at a surface point [58]. It is now easy to see that the integrand of Eq. (6) peaks in the region  $|\mathbf{s} - \mathbf{s}'| \lesssim$

$(k_{\epsilon+\hbar\omega} - k_\epsilon)^{-1}$  and rapidly oscillates outside of it. For  $\epsilon \sim E_F$  and  $\hbar\omega/E_F \ll 1$ , this sets the scale  $|\mathbf{s} - \mathbf{s}'| \sim v_F/\omega$  for the  $e$ - $h$  correlation function  $F_\omega(\mathbf{s}, \mathbf{s}')$  in Eq. (5). Finally, for  $L \gg v_F/\omega$ , after computing normal derivatives in  $\rho_{nn'}(\epsilon; \mathbf{s}, \mathbf{s}') = 2\nabla_n \nabla_{n'} \text{Im}G_0(\epsilon, \mathbf{s} - \mathbf{s}')$  relative to the tangent plane at a surface point [58], we obtain  $\bar{F}_\omega = (2m^4 E_F^2 / \pi \hbar^8) \hbar\omega$ , yielding Eq. (1).

The surface contribution  $Q_s$  to the full absorbed power  $Q$  should be considered in conjunction with its bulk counterpart  $Q_0$ , i.e.,  $Q = Q_0 + Q_s$ . The bulk contribution is given by the standard expression (2), where the metal dielectric function  $\epsilon(\omega)$  includes only the bulk processes. In the following, we adopt the Drude dielectric function  $\epsilon(\omega) = \epsilon_i(\omega) - \omega_p^2/\omega(\omega + i\gamma)$ , where  $\epsilon_i(\omega)$  describes interband transitions,  $\omega_p$  is the plasma frequency, and  $\gamma$  is the scattering rate. In fact, both bulk and surface contributions can be combined, in a natural way, within the general expression (2). Indeed, using the relation  $\omega_p^2 = 16e^2 E_F^2 / 3\pi \hbar^3 v_F$ , the surface absorbed power (1) can be recast as

$$Q_s = \frac{3v_F \omega_p^2}{32\pi \omega^2} \int dS |E_n|^2. \quad (8)$$

Then, it is easy to see that the surface contribution can be incorporated into general expression (2) for the absorbed power by modifying the Drude scattering rate as  $\gamma = \gamma_0 + \gamma_s$ , where  $\gamma_0$  is the usual bulk scattering rate and

$$\gamma_s = \frac{3v_F}{4} \frac{\int dS |E_n|^2}{\int dV |\mathbf{E}|^2}, \quad (9)$$

is the surface scattering rate. Indeed, after this modification,  $Q_s$  can be obtained from Eq. (2) as the first-order expansion term in  $\gamma_s$ , indicating that the surface scattering mechanism should be treated on par with phonon and impurity scattering. Note that  $\gamma_s$  is independent of the local field overall strength but highly sensitive to its polarization relative to the metal-dielectric interface.

Turning to the surface-assisted plasmon decay (Landau damping), the plasmon decay rate in any metal-dielectric structure is given by general expression [60]  $\Gamma = Q/U$ , where  $U$  is the plasmon energy [57],

$$U = \frac{\omega}{16\pi} \frac{\partial \epsilon'(\omega)}{\partial \omega} \int dV |\mathbf{E}|^2. \quad (10)$$

Using Eq. (2) for the absorbed power, the decay rate has the standard form,

$$\Gamma = 2\epsilon''(\omega) \left[ \frac{\partial \epsilon'(\omega)}{\partial \omega} \right]^{-1}. \quad (11)$$

Let us show that the full plasmon decay rate that includes both bulk and surface contributions is given by Eq. (11), but with  $\epsilon(\omega)$  modified according to Eq. (9). Indeed, using Eq. (8), the surface contribution to  $\Gamma$  takes the form

$$\Gamma_s = \frac{Q_s}{U} = \frac{2\omega_p^2 \gamma_s}{\omega^3} \left[ \frac{\partial \epsilon'(\omega)}{\partial \omega} \right]^{-1}, \quad (12)$$

where  $\gamma_s$  is given by Eq. (9). The same expression is obtained, in the first order in  $\gamma_s$ , from Eq. (11) with surface-modified  $\varepsilon(\omega)$ . Note that for  $\omega$  well below the interband transitions onset, the plasmon decay rate and scattering rate coincide,  $\Gamma \approx \gamma = \gamma_0 + \gamma_s$ .

### III. APPLICATIONS

Let us now discuss the effect of field polarization and system geometry on the carrier excitation efficiency. The surface enhancement factor of the absorbed power is given by the ratio of full ( $Q$ ) to bulk ( $Q_0$ ) absorbed power,  $M = Q/Q_0$ , which, within RPA, takes a simple form

$$M = 1 + \frac{\gamma_s}{\gamma_0}. \quad (13)$$

Evaluation of surface scattering rate  $\gamma_s$  is made more convenient by noting that the Gauss's law reduces the volume integral in Eq. (9) to the surface term, so that

$$\gamma_s = A v_F \frac{\int dS |\nabla_n \Phi|^2}{\int dS \Phi^* \nabla_n \Phi}, \quad (14)$$

where real part of the denominator is implied. This form of  $\gamma_s$  as the ratio of two surface integrals reflects the fact that  $e$ - $h$  pairs are excited in a close proximity (within  $v_F/\omega$ ) to the interface. The constant  $A$ , which equals  $A = 3/4$  for the hard-core confining potential, can be determined by matching Eq. (14) with the corresponding rate for a spherical particle with radius  $a$ . A straightforward evaluation of Eq. (14) recovers the standard result for a sphere  $\gamma_{sp} = A v_F/a$ , while in the recent TDLDA calculations for relatively large (up to  $a = 10$  nm) spherical particles [45, 46] the value  $A \approx 0.32$  was obtained. Note that for systems, whose geometry permits separation of variables, the form (14) of  $\gamma_s$  is especially useful since it leads to *analytical* results for some common structures that so far eluded attempts of any quantum-mechanical evaluation, as we illustrate below for metal nanorods and nanodisks.

In Figs. 1 and 2, we show calculated surface scattering rates for nanorods and nanodisks, which are modeled here by prolate and oblate spheroidal nanoparticles, respectively. These structures support longitudinal and transverse plasmon modes oscillating along the symmetry axis (semi-axis  $a$ ) and within the symmetry plane (semi-axis  $b$ ). Using Eq. (14),  $\gamma_s$  for all modes can be found in an analytical form [58], but here only the results for the dipole mode are presented. For a nanorod (prolate spheroid) with the aspect ratio  $b/a < 1$ , we obtain  $\gamma_s = \gamma_{sp} f_{L,T}$ , where

$$f_L = \frac{3}{2 \tan^2 \alpha} \left[ \frac{2\alpha}{\sin 2\alpha} - 1 \right], \quad f_T = \frac{3}{4 \sin^2 \alpha} \left[ 1 - \frac{2\alpha}{\tan 2\alpha} \right], \quad (15)$$

are the normalized rates for longitudinal and transverse modes relative to the spherical particle rate, and  $\alpha =$

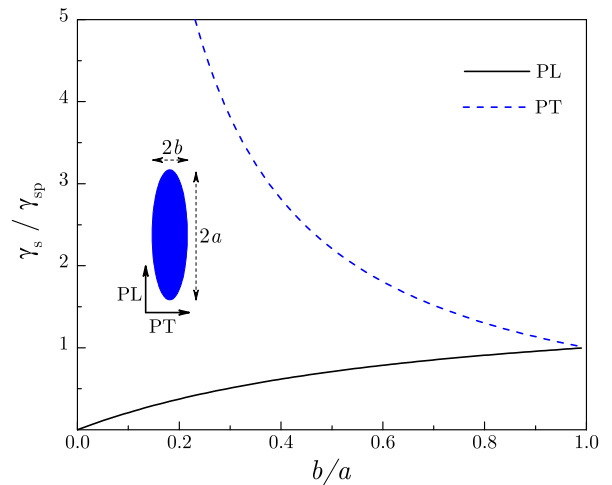


FIG. 1. Normalized rates for longitudinal and transverse dipole modes in prolate spheroidal particles (nanorods) relative to the spherical particle rate are shown with changing aspect ratio  $b/a$ . Inset: Schematics for the mode polarizations.

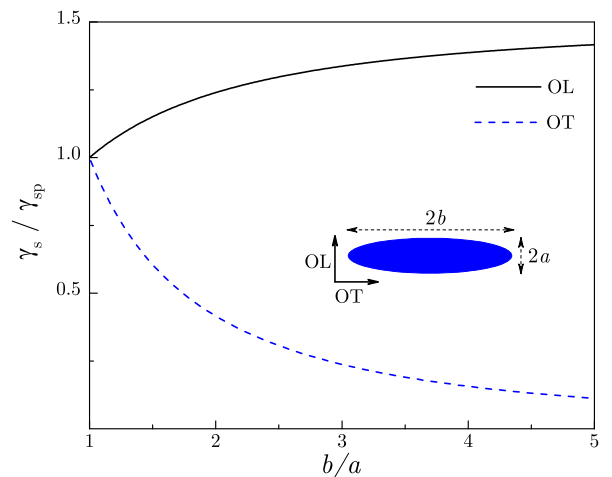


FIG. 2. Normalized rates for longitudinal and transverse dipole modes in oblate spheroidal particles (nanodisks) relative to the spherical particle rate are shown with changing aspect ratio  $b/a$ . Inset: Schematics for the mode polarizations.

$\arccos(b/a)$  is the angular eccentricity. For a nanodisk (oblate spheroid) with  $b/a > 1$ , the normalized rates have the same form (15) but with  $\alpha = i \operatorname{arccosh}(b/a)$ . In Fig. 1, we show the normalized rates in a prolate spheroid ( $b/a < 1$ ) for both longitudinal (PL) and transverse (PT) modes as the system shape evolves from a needle to a sphere. With changing aspect ratio  $b/a$ , the rates exhibit a dramatic difference in behavior depending on the local field polarization. As nanorods become thinner, the normalized rate decreases for the PL mode but increases for the PT modes. These trends are reversed for nanodisks ( $b/a > 1$ ), shown in Fig. 2: the normalized rates increase for the longitudinal (OL) mode and decrease for the transverse OT mode as the nanodisk radius increases (at fixed height).

The dominant factor that determines the surface en-

hancement of carrier excitation efficiency is the local field polarization relative to the metal-dielectric interface. In a given system, the surface-assisted carrier excitation rate can be manipulated in a wide range by choosing the electric field orientation. Note that recent measurements [32] of plasmon spectra in cylinder-shaped nanorods and nanodisks revealed strong polarization dependence of plasmon linewidth.

#### IV. CONCLUSIONS

In summary, we developed a quantum-mechanical model for surface-assisted carrier excitation in plasmonic

nanostructures of arbitrary shape. We derived explicit expressions for surface absorbed power and scattering rate that are highly sensitive to the local field polarization relative to the metal-dielectric interface. Our results can be used for calculations of hot carrier generation rates in photovoltaics and photochemistry applications [1].

#### ACKNOWLEDGMENTS

This work was supported in part by the National Science Foundation under grants No. DMR-1610427 and No. HRD-1547754.

- 
- [1] M. L. Brongersma, N. J. Halas, and P. Nordlander, *Nat. Nanotechnol.* **10**, 25 (2015).
  - [2] Y. K. Lee, C. H. Jung, J. Park, H. Seo, G. A. Somorjai, and J. Y. Park, *Nano Lett.* **11**, 4251 (2011).
  - [3] F. Wang and N. A. Melosh, *Nano Lett.* **11**, 5426 (2011).
  - [4] M. W. Knight, H. Sobhani, P. Nordlander, and N. J. Halas, *Science* **332**, 702 (2011).
  - [5] A. Sobhani, M. W. Knight, Y. Wang, B. Zheng, N. S. King, L. V. Brown, Z. Fang, P. Nordlander, and N. J. Halas, *Nat. Commun.* **4**, 1643 (2013).
  - [6] K. Wu, W. E. Rodriguez-Cordoba, Y. Yang, and T. Lian, *Nano Lett.* **13**, 5255 (2013).
  - [7] M. W. Knight, Y. Wang, A. S. Urban, A. Sobhani, B. Y. Zheng, P. Nordlander, and N. J. Halas, *Nano Lett.* **13**, 1687 (2013).
  - [8] C. Clavero, *Nat. Photonics* **8**, 95 (2014).
  - [9] H. Chalabi, D. Schoen, M. L. Brongersma, *Nano Lett.* **14**, 1374 (2014).
  - [10] R. Sundararaman, P. Narang, A. S. Jermyn, W. A. Goddard III, and H. A. Atwater, *Nat. Commun.* **5**, 5788 (2014).
  - [11] B. Y. Zheng, H. Zhao, A. Manjavacas, M. McClain, P. Nordlander, and N. J. Halas, *Nat. Commun.* **6**, 7797 (2015).
  - [12] I. Thomann, B. A. Pinaud, Z. Chen, B. M. Clemens, T. F. Jaramillo, and M. L. Brongersma, *Nano Lett.* **11**, 3440 (2011).
  - [13] J. Lee, S. Mubeen, X. Ji, G. D. Stucky, and M. Moskovits, *Nano Lett.* **12**, 5014 (2012).
  - [14] S. Mukherjee, F. Libisch, N. Large, O. Neumann, L. V. Brown, J. Cheng, J. B. Lassiter, E. A. Carter, P. Nordlander, and N. J. Halas, *Nano Lett.* **13**, 240 (2013).
  - [15] S. Mubeen, J. Lee, N. Singh, S. Krämer, G. D. Stucky, and M. Moskovits, *Nat. Nanotechnol.* **8**, 247 (2013).
  - [16] S. Mukherjee, L. Zhou, A. M. Goodman, N. Large, C. Ayala-Orozco, Y. Zhang, P. Nordlander, and N. J. Halas, *J. Am. Chem. Soc.* **136**, 64 (2014).
  - [17] W. P. Halperin, *Quantum size effects in metal particles*, *Rev. Mod. Phys.* **58**, 533 (1986).
  - [18] V. V. Kresin, *Phys. Rep.* **220**, 1 (1992).
  - [19] C. Voisin, N. Del Fatti, D. Christofilos, and F. Vallée, *J. Phys. Chem. B* **105**, 2264 (2001).
  - [20] K. L. Kelly, E. Coronado, L. L. Zhao, and G. C. Schatz, *J. Phys. Chem. B* **107**, 668 (2003).
  - [21] C. Noguez, *J. Phys. Chem. C* **111**, 3806 (2007).
  - [22] T. Klar, M. Perner, S. Grosse, G. von Plessen, W. Spirkel, and J. Feldmann, *Phys. Rev. Lett.* **80**, 4249 (1998).
  - [23] C. Sönnichsen, T. Franzl, T. Wilk, G. von Plessen, J. Feldmann, O. V. Wilson, and P. Mulvaney, *Phys. Rev. Lett.* **88**, 077402 (2002).
  - [24] S. L. Westcott, J. B. Jackson, C. Radloff, and N. J. Halas, *Phys. Rev. B* **66**, 155431 (2002).
  - [25] G. Raschke, S. Brogl, A. S. Susha, A. L. Rogach, T. A. Klar, and J. Feldmann, *Nano Lett.* **4**, 1853 (2004).
  - [26] A. Arbouet, D. Christofilos, N. Del Fatti, F. Vallée, J. R. Huntzinger, L. Arnaud, P. Billaud, and M. Broyer, *Phys. Rev. Lett.* **93**, 127401 (2004).
  - [27] C. L. Nehl, N. K. Grady, G. P. Goodrich, F. Tam, N. J. Halas, and J. H. Hafner, *Nano Lett.* **4**, 2355 (2004).
  - [28] C. Novo, D. Gomez, J. Perez-Juste, Z. Zhang, H. Petrova, M. Reismann, P. Mulvaney, and G. V. Hartland, *Phys. Chem. Chem. Phys.* **8**, 3540 (2006).
  - [29] H. Baida, P. Billaud, S. Marhaba, D. Christofilos, E. Cottancin, A. Crut, J. Lermé, P. Maioli, M. Pellarin, M. Broyer, N. Del Fatti, and F. Vallée, *Nano Lett.* **9**, 3463 (2009).
  - [30] M. G. Blaber, A.-I. Henry, J. M. Bingham, G. C. Schatz, and R. P. Van Duyne, *J. Phys. Chem. C* **116**, 393 (2012).
  - [31] V. Juvé, M. F. Cardinal, A. Lombardi, A. Crut, P. Maioli, J. Pérez-Juste, L. M. Liz-Marzán, N. Del Fatti, and F. Vallée, *Nano Lett.* **13**, 2234 (2013).
  - [32] M. N. O'Brien, M. R. Jones, K. L. Kohlstedt, G. C. Schatz, and C. A. Mirkin, *Nano Lett.* **15**, 1012 (2015).
  - [33] A. Kawabata and R. Kubo, *J. Phys. Soc. Jpn.* **21**, 1765 (1966).
  - [34] A. A. Lushnikov and A. J. Simonov, *Z. Physik* **270**, 17 (1974).
  - [35] W. A. Kraus and G. C. Schatz, *J. Chem. Phys.* **79**, 6130 (1983).
  - [36] M. Barma and V. J. Subrahmanyam, *J. Phys.: Cond. Mat.* **1**, 7681 (1989).
  - [37] C. Yannouleas and R. A. Broglia, *Ann. Phys.* **217**, 105 (1992).
  - [38] M. Eto and K. Kawamura, *Surf. Rev. Lett.* **3**, 151 (1996).
  - [39] A. V. Uskov, I. E. Protsenko, N. A. Mortensen, and E. P. O'Reilly, *Plasmonics* **9**, 185 (2013).
  - [40] J. B. Khurgin and G. Sun, *Opt. Exp.* **23**, 250905 (2015).

- [41] A. S. Kirakosyan, M. I. Stockman, and T. V. Shahbazyan, Phys. Rev. B **94**, 155429 (2016).
- [42] R. A. Molina, D. Weinmann, and R. A. Jalabert, Phys. Rev. B **65**, 155427 (2002).
- [43] G. Weick, R. A. Molina, D. Weinmann, and R. A. Jalabert, Phys. Rev. B **72**, 115410 (2005).
- [44] Z. Yuan and S. Gao, Surf. Sci. **602**, 440 (2008).
- [45] J. Lermé, H. Baida, C. Bonnet, M. Broyer, E. Cottancin, A. Crut, P. Maioli, N. Del Fatti, F. Vallée, and M. Pellarin, J. Phys. Chem. Lett. **1**, 2922 (2010).
- [46] J. Lermé, J. Phys. Chem. C **115**, 14098 (2011).
- [47] X. Li, Di Xiao, and Z. Zhang, New J. Phys. **15**, 023011 (2013).
- [48] A. Manjavacas, J. G. Liu, V. Kulkarni, and P. Nordlander, ACS Nano **8**, 7630 (2014).
- [49] L. Genzel, T. P. Martin, and U. Kreibig, Z. Phys. B **21**, 339 (1975).
- [50] R. Ruppin and H. Yatom, Phys. Status Solidi **74**, 647 (1976).
- [51] W. A. Krauss and G. C. Schatz, Chem. Phys. Lett. **99**, 353 (1983).
- [52] E. A. Coronado and G. C. Schatz, J. Chem. Phys. **119**, 3926 (2003).
- [53] A. Moroz, J. Phys. Chem. C **112**, 10641 (2008).
- [54] U. Kreibig and M. Vollmer, *Optical Properties of Metal Clusters* (Springer, Berlin, 1995).
- [55] N. A. Mortensen, Photonic. Nanostruct. **11**, 303 (2013).
- [56] N. A. Mortensen, S. Raza, M. Wubs, T. Sondergaard, and S. I. Bozhevolnyi, Nat. Commun. **5**, 3809 (2014).
- [57] L. D. Landau and E. M. Lifshitz, *Electrodynamics of Continuous Media* (Elsevier, Amsterdam, 2004).
- [58] T. V. Shahbazyan, Phys. Rev. B **94**, 235431 (2016).
- [59] R. Balian and C. Bloch, Ann. Phys. **60**, 401 (1970).
- [60] T. V. Shahbazyan, Phys. Rev. Lett. **117**, 207401 (2016).